

SPECTRAL CHARACTERIZATION OF LONGITUDINAL COUPLED-BUNCH INSTABILITIES AT THE ADVANCED LIGHT SOURCE

J.M. BYRD and J. CORLETT

*Lawrence Berkeley Laboratory, One Cyclotron Road,
Berkeley, California 94720, USA*

(Received 21 January 1995; in final form 22 May 1995)

We present the results of an experimental study of longitudinal coupled-bunch (CB) motion observed in the newly commissioned Advanced Light Source (ALS). Our study identifies the frequencies of the monopole higher-order modes (HOMs) of the RF cavities driving the beam by correlating the frequencies of the beam oscillations for different symmetric beam filling patterns with the measured cavity HOM frequencies. Self-limiting of the largest coherent coupled-bunch oscillation occurs at ~ 10 degrees at the RF frequency with an individual bunch amplitude of no greater than 20–30 degrees, depending on the total beam current. A qualitative discussion of a limiting mechanism to CB growth is presented along with computer tracking studies.

KEY WORDS: Collective effects, impedances, instabilities, particle dynamics, storage rings

1 INTRODUCTION

The demand for high-current electron storage rings for use as flavor factories or as synchrotron light sources has led to the use of many bunches to avoid single bunch current limits, sometimes filling all radiofrequency (RF) buckets around the ring. For these storage rings, coupled-bunch instabilities present one of the challenges to successful operation by degrading beam quality in terms of lifetime, luminosity, or beamsize. The Advanced Light Source (ALS), a 1.5 GeV electron storage used for the production of high brightness synchrotron radiation, is such a ring. Selected ALS parameters are listed in Table 1.

The ALS was recently constructed at Lawrence Berkeley Laboratory. Beam was first stored in the ALS in March 1993, and the facility is currently providing beam for experimental users. The storage ring beam current has reached 470 mA, surpassing the 400 mA design goal with no indication of limitation of the current from beam instability. However, strong dipole coupled-bunch (CB) oscillations in the longitudinal and transverse directions have been observed.¹ The longitudinal oscillations are large enough that they degrade the quality of the synchrotron radiation used by experimenters in two ways:

TABLE 1: ALS storage ring parameters.

Parameter	Description	Value
E	Beam energy	1.5 GeV
C	Circumference	196.8 m
f_{rf}	RF Freq.	499.654 MHz
σ_e	RMS $\delta E/E$	7.1e-4
h	Harmonic Number	328
I_0	Design beam current	0.4 A
α	momentum compaction	1.594e-3
Q_s	Synchrotron tune	0.006
σ_ℓ	RMS bunch length	6 mm
τ_{rad}	longitudinal damping time	13.5 msec

- (1) an effective increase in the average horizontal beam size at dispersive regions in the storage ring lattice and
- (2) increased spectral width of the light in higher harmonics of insertion devices.² The oscillations are presently one of the limiting factors in achieving the original design parameters of the storage ring. Longitudinal and transverse feedback systems are being commissioned to damp the oscillations.

We report here the results of an experimental study characterizing the longitudinal CB motion. We identify the resonant modes of the RF cavities by RF measurement of a spare cavity in the laboratory and correlate these with HOMs driving the beam, and measure the oscillation amplitudes of all coupled beam modes as a function of current. Because the longitudinal instability threshold occurs at relatively low beam current (<10 mA), we have been able to study the evolution of the unstable beam over a wide range of beam currents. This may give insight into the study of the limiting mechanism in other electron or positron storage rings.

2 LONGITUDINAL COUPLED-BUNCH INSTABILITIES

Collective instabilities of bunched beams in high-energy storage rings have been studied extensively for some time.³ In the case of CB instabilities, an electron bunch passing through the storage ring vacuum chamber excites currents in the chamber walls which in turn excite electromagnetic fields which can act back on consecutive bunches. The wake field expresses the net voltage per unit charge on a subsequent test charge from the induced electromagnetic fields. Although the wake field can be of a general form, for the longitudinal CB motion

we need only consider the wakefields generated by the modes of a resonant structure such as an RF cavity. If the cavity wake fields persist until the next bunch passage, they couple the longitudinal (or transverse) oscillations of the bunches. Under certain conditions the coupling results in an instability in which the relative motion of the bunches form a coherent oscillation whose amplitude grows exponentially until either the beam reaches a limiting aperture and the total current drops below the instability threshold, or a mechanism such as linear or nonlinear Landau damping limits further growth.^{4,5}

The stability of the system of CB oscillations can be determined using a normal-modes approach.⁶ The simplest situation is for a beam of N identical bunches equally spaced around the ring. In this case, the N normal modes of oscillation in the longitudinal direction can be described by a relative instantaneous phase in the oscillation of each successive bunch given by Ref. 3

$$\Delta\phi = \frac{2\pi}{N} \ell \quad (1)$$

where ℓ is the mode index and ranges from 0 to $N - 1$. It can be shown that the exponential growth rate of CB mode ℓ is given by

$$\frac{1}{\tau} = \frac{1}{2} f_0 \frac{I_0 h \alpha}{(E/e) Q_s} \operatorname{Re}[Z_{\parallel}]_{\text{eff}}^{\ell} \quad (2)$$

where

$$[Z_{\parallel}]_{\text{eff}}^{\ell} = \sum_{p=-\infty}^{p=+\infty} \frac{\omega_p}{\omega_r f} e^{-(\omega_p \sigma_{\tau})^2} Z_{\parallel}(\omega_p) \quad (3)$$

and

$$\omega_p = (pN + \ell + Q_s)\omega_0. \quad (4)$$

The effective impedance, $[Z_{\parallel}]_{\text{eff}}$, represents the sum of the RF cavity resonant mode impedance weighted by the single bunch spectrum. Because the length of the bunch in the ALS is small compared to the wavelength of the the known HOM fields driving coupled oscillations, we treat it here as pointlike. The condition for a beam instability occurs when the growth rate exceeds the sum of the natural damping mechanisms such as radiation damping and Landau damping. All beam measurements were restricted to symmetric fill patterns because of the relative simplicity of the normal modes.

The impedance of each cavity mode is of the form

$$Z_{\parallel}(\omega) = \frac{R_s}{1 + jQ\left(\frac{\omega}{\omega_r} - \frac{\omega_r}{\omega}\right)} \quad (5)$$

where R_s is the shunt impedance of the mode, Q is the quality factor, and ω_r is the resonant frequency. Measurements of the ALS RF cavity are discussed in Section 3.

Note that the growth rate only applies at the onset of the instability. Some theoretical and numerical studies have been made to explore the long-term development of the unstable

beam, focussing on the effects of linear and nonlinear Landau damping within the bunch.⁷ As of yet there is no general understanding of the limiting mechanisms of CB oscillations and no means for predicting the limiting amplitudes. A qualitative discussion of a relatively novel mechanism which may apply to the case of the ALS is presented in Section 5.

3 RF CAVITY MEASUREMENTS

3.1 RF System Design

The two 500 MHz RF cavities in the ALS are fed from a single klystron through waveguide with aperture coupling to the cavities.⁸ The use of aperture coupling has the advantage of allowing some of the higher order modes (HOMs) to be coupled into the feeder waveguide, giving an effective damping mechanism. To improve this damping a pair of bifurcated waveguide filters (high pass) are installed in the waveguide feeding each cavity, one E-plane and one H-plane. Absorptive loads are placed at the ends of these filters to absorb any high frequency power coupled from cavity HOMs and passed by the filters, thereby reducing the Q value of those HOMs. A similar arrangement is used in the matching waveguide, to allow further damping of HOM's coupled into the waveguide. Cavity tuning is accomplished by use of a copper plunger driven into or out of the cavity. Cavity temperature is controlled by water flowing inside an outer jacket containing the cavity body.

3.2 Cavity Measurements

We measured the HOMs in a spare cavity to determine their resonant frequencies and Q values. The cavity was connected to a waveguide section using a side-coupled aperture of the same design as that used in the ALS. Bifurcated sections were placed at the ends of the waveguide, followed by absorptive ferrite tiles. A cylindrical alumina window was included in the coupling aperture to simulate ALS operational conditions. HOM's were excited by E-field probes inserted into the cavity beampipes. Q determinations were made from 3-dB point measurements of transmission from probe to probe through the cavity (S_{21}) with minimal loading of the resonance by the measurement probes. As an aid to mode identification, the perturbation in resonant frequency was measured as a needle was pulled through the cavity on a nylon thread, at various offsets from the centerline. Observation of the perturbation profile as a function of position in the cavity allowed identification of modes in terms of azimuthal and longitudinal electric field distributions, which was then used with the frequency measurement to correlate modes with URMEL results. For the higher frequency modes close to the beam pipe cutoff frequency of 3 GHz, Q values are somewhat inaccurate because of the termination of the short beam pipes in the experimental measurements. Once identified in this manner, we used the measured Q values and the R/Q computed by URMEL to determine the shunt impedance of all HOMs. The HOM resonant frequencies and shunt impedances are shown in Table 2.⁹ Although there may be variations between actual and computed R/Q values, we expect these to be small.

For the strongest HOM's we measured variation in frequency with cavity temperature, by adjusting the temperature of the cooling water flowing in the jacket surrounding

TABLE 2: Strongest RF cavity monopole HOM's.

f_r (MHz)	Q	R_s (k Ω)	$\Delta f/\Delta T$ (kHz/C)	$\Delta f/\Delta x_{\text{tuner}}$ (kHz/mm)
808.44	21000	1050	-20	37
1275.1	3000	33	-45	276
1553.55	3400	26.5	-28	-118
2853.75	4000	18.8	-32	-6
2353	5100	16.8	-31	-35
1807.68	2900	13.3	-33	
3260	1500	12.1		
3260	1500	11.5		
2488.94	2400	8.4	19	
2124.61	1800	7.6	10	-155

the cavity. We also measured the frequency shift of the strongest HOM's as a function of tuner position. These results are summarized in Table 2.

4 BEAM CHARACTERIZATION MEASUREMENTS

4.1 Beam Spectrum

Beam oscillations were measured using pickup electrodes located at a single point in the ring. The pickup signal used was the sum of four beam position button-type electrodes located azimuthally around the vacuum chamber. To first order, the sum signal does not contain any transverse position information and thus any modulation of the signal results from time or phase modulation of the beam. The signal was not conditioned in any way except via the summing process and the ~ 130 meter cable carrying the signal to the control room. All observed beam signals resulted from spontaneous self-excitation of the beam. We attribute this to be from CB oscillations.

To simplify interpretation of the beam spectrum, we used filling patterns of equally populated and equally spaced bunches. For a symmetric fill pattern of N bunches, the signal from an ideal pickup is a series of delta function impulses given by Ref. 11

$$s(t) = 2k_{pu}q \sum_{n=-\infty}^{\infty} \sum_{m=1}^N \delta \left(t - nT_0 - m \frac{T_0}{N} - \tau_m \cos(\omega_s t + \phi_m) \right) \quad (6)$$

where q is the bunch charge, k_{pu} is the loss parameter of the pickup, τ_m the oscillation amplitude of bunch m in units of time, ω_s the angular synchrotron frequency, and ϕ_m the

relative phase of oscillation of bunch m . The summations are over bunch number m and turn number n . The pickup signal in the frequency domain can be expressed as

$$s(\omega) = 2k_{puq} \sum_{l=0}^{N-1} \sum_{k=-\infty}^{\infty} (-j)^k J_k(\omega\tau_l) \sum_{p=-\infty}^{\infty} \delta(\omega - pN\omega_0 - k(l + Q_s)\omega_0) \quad (7)$$

where τ_l is the oscillation amplitude of CB mode l in units of time, and J_k is the k th order Bessel function. At the frequencies used in the measurements, the bunch can be considered a point charge.

Observed on a spectrum analyzer, the beam current spectrum has frequency components at multiples of the bunch frequency, Nf_0 , with an amplitude proportional to the total beam current. The oscillations of individual CB modes appear as phase modulation (PM) sidebands about the bunch harmonics where $pNf_0\tau_l$ is the amplitude of PM. The first order sideband appears at frequencies $pNf_0 \pm (\ell f_0 + f_s)$. The beam spectrum for the case of 3 equally spaced bunches is illustrated in Figure 1. The oscillation amplitude of CB mode ℓ can be determined from the ratio of the PM sidebands. We used the ratio of the first order sideband to the carrier which is the most sensitive. Note that all N CB modes can be measured in a frequency span of pNf_0 to $pNf_0 + \frac{Nf_0}{2}$ or from $pNf_0 + \frac{Nf_0}{2}$ to $(p+1)Nf_0$. For example, in the case of a bunch in every RF bucket, all CB modes appear in each of the frequency spans 0–250 MHz, 250–500 MHz, 500–750 MHz, etc.

In our measurements, the storage ring was filled in symmetric patterns of 82 (every 4th RF bucket) and 328 (all RF buckets) bunches and the amplitudes of all longitudinal CB modes were measured as a function of current. Unavoidable variations in the charge of each bunch led to small frequency components at revolution harmonics between bunch harmonics. These were used as a measure of the uniformity of the fill pattern. We observed 1–5% variations in the bunch uniformity around the ring. The process of recording the sidebands of many revolution harmonics from the spectrum analyzer was automated by way of a MacIntosh computer equipped with a GPIB interface.

Shown in Figure 2 are some representative beam spectra for the case of 82 bunches showing the CB mode oscillations which appear as upper or lower sidebands of the revolution harmonics. The measurements were made in the frequency band 500–562.5 MHz. The number of revolution harmonics away from the main bunch harmonic at 500 MHz is indicated in each spectrum. The center peak corresponds to an orbit harmonic. Except for the main bunch harmonic, these orbit harmonics result from an unavoidable slight asymmetry in the bunch charges. The sidebands are first order PM sidebands spaced by f_s from the revolution harmonics. The sidebands at $2f_s$ are second-order PM sidebands. The amplitude of all CB modes for the 328 and 82 bunch configurations at several beam currents are shown in Figures 3 and 4. The oscillation amplitudes are expressed in degrees of phase modulation at the RF frequency, 500 MHz.

The suggestive patterns observed in the CB modes can most easily be understood by comparing them with the effective impedance, $[Z_{\parallel}]_{\text{eff}}$, given in Equation 3 for a given bunch filling pattern evaluated using the measured parameters of the RF cavity HOMs. In this case, it is more instructive to evaluate the impedance as a continuous function of CB mode frequency rather than the discrete set of mode frequencies. The real part of $[Z_{\parallel}]_{\text{eff}}$ for the 328 and 82 bunch case is shown in Figures 3c and 4b, respectively.

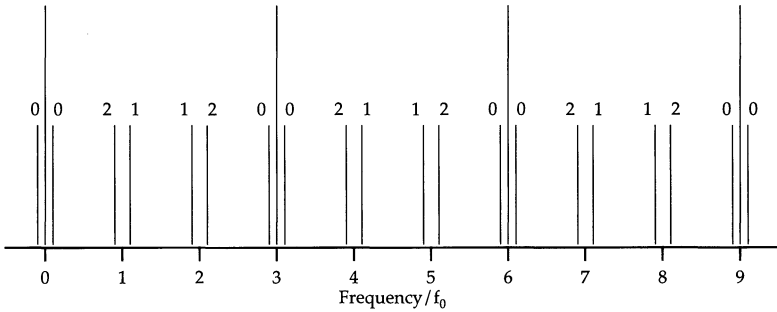


FIGURE 1: Beam spectrum for 3 equally spaced bunches. Signals proportional to the total current appear at the bunch harmonic frequencies with coupled-bunch oscillations appearing as phase modulation sidebands.

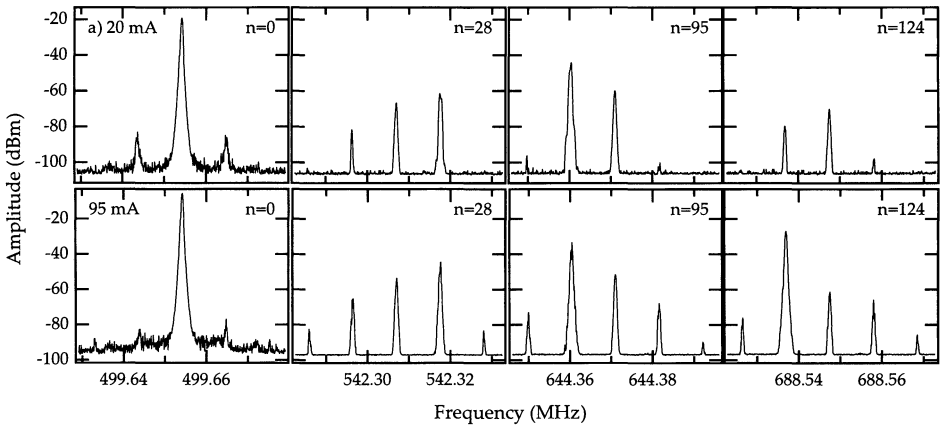


FIGURE 2: Raw frequency spectra near selected revolution harmonics. The number of revolution harmonics (n) from the RF frequency is indicated in each plot. The top row is measured at 20 mA and the bottom at 95 mA of total beam current.

The left axis is the effective impedance and the right axis the corresponding growth rate at 20 mA. The dotted line represents the effective impedance resulting in growth for CB modes corresponding to upper sidebands in the frequency range. The dashed line is the effective impedance resulting in growth for lower sidebands in the same frequency range. Note that the dashed line represents a damping impedance for the upper sideband modes in the same frequency range and the dotted line a damping impedance for lower sideband modes. The aliased HOM's are labeled according to their resonant frequency as given in Table 2. The radiation damping rate is also shown.

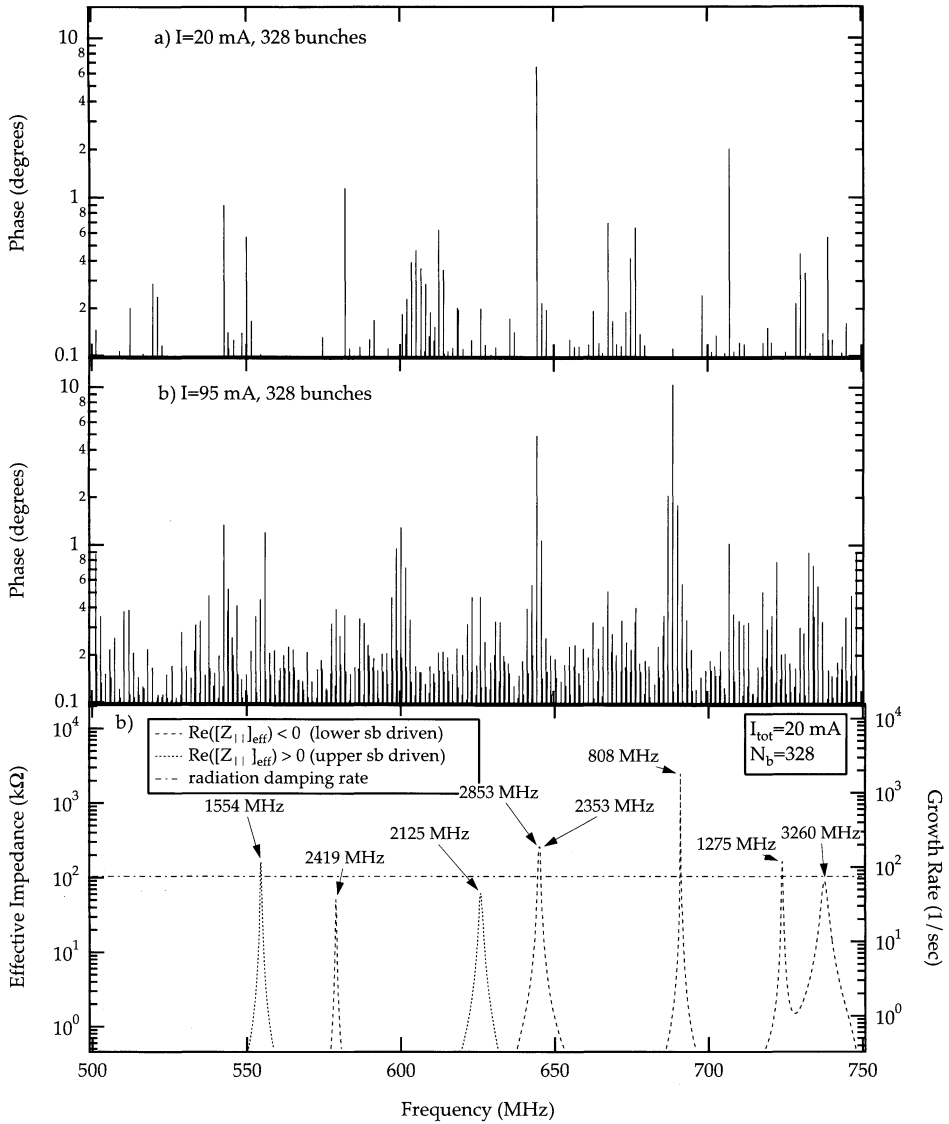


FIGURE 3: (a–b) Measured spectrum of first-order longitudinal sidebands for 328 bunches in the frequency range 500–750 MHz for 20 and 95 mA. (c) Real part of the RF cavity impedance aliased into the same frequency range. The corresponding growth rate for 20 mA is shown on the right axis.

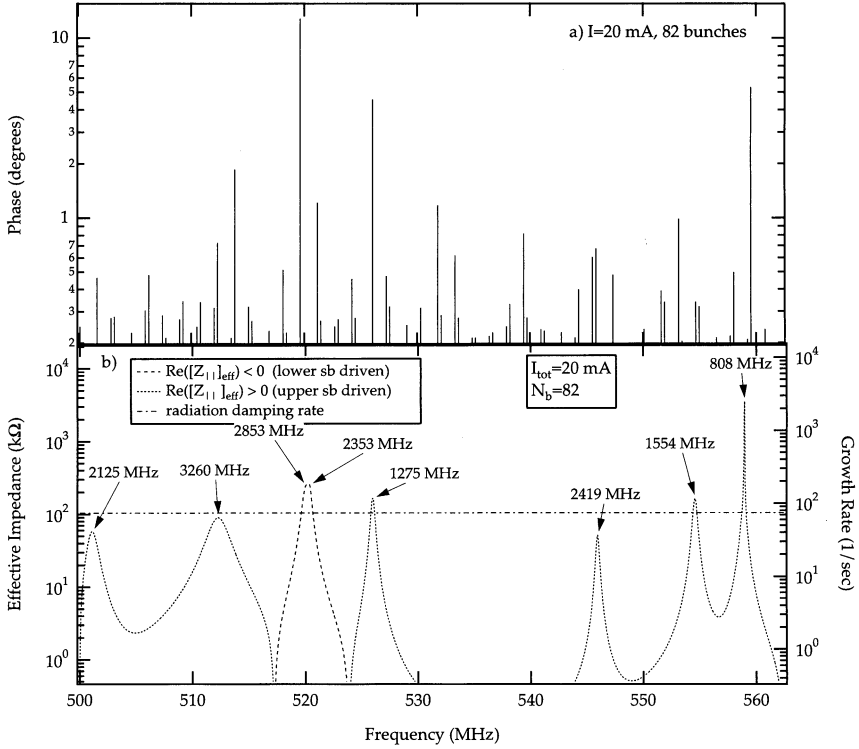


FIGURE 4: (a–b) Measured spectrum of first-order longitudinal sidebands for 82 bunches in the frequency range 500–625 MHz for 20 mA. (c) Real part of the RF cavity impedance aliased into the same frequency range. The corresponding growth rate for 20 mA is shown on the right axis.

Comparing the effective impedance with the CB mode amplitudes for each filling pattern, we can correlate the CB mode spectrum with the measured impedance and positively identify the strongest driving HOMs. Consider the mode spectrum for the 328 bunch pattern. At 95 mA, the strongest CB modes are driven by the high- Q TM-011 mode ($f_r = 808$ MHz) and the next strongest CB modes by the modes at 2.3 and 2.8 GHz. At 20 mA, the high- Q mode has no effect. We believe the difference in the CB mode spectrum between the two current levels to result from the HOM frequency dependence on RF cavity temperature and tuner position. The narrow bandwidth of the high- Q mode (40 kHz) could allow the HOM frequency to be tuned between CB modes frequencies and have no effect on beam stability at 20 mA. Tuner variations are believed to have shifted the frequency of the HOM onto or near a CB mode at 95 mA. Subsequent experiments changing the cavity temperature and tuner position have shown that the stability of this CB mode changes greatly with cavity conditions whereas the effect on the the 2.3 and 2.8 GHz HOMs is such that the growth rates are reduced but not eliminated. This is consistent with our measurement of the HOM frequency dependence on temperature and tuner position.

For the 82 bunch filling pattern, the largest CB mode, which appears as a lower sideband at ~ 519 MHz in this frequency band, is driven by the combined effect of HOMs at 2.3 and 2.8 GHz. The next largest CB mode, which appears as an upper sideband at ~ 558 MHz in this frequency band, is driven by the high- Q TM-011 mode.

Unfortunately, it is difficult to accurately determine the exact frequencies of all HOMs as cavity conditions change. Some HOM's couple to cavity or waveguide probes, however the strongest high- Q modes are trapped within the cavity and are weakly coupled to available probes. We were able to measure the frequencies of the strongest HOMs to within 1.52 MHz (the revolution frequency) by observing beam-induced signals in each cavity. We attribute lack of correlation of some the weaker HOMs with CB modes to this difficulty. However, it is possible that there is another source of impedance in the vacuum chamber.

Individual modes grow in amplitude as a function of beam current, limiting at a phase excursion of approximately 10 degrees at 500 MHz. As the current increases, other modes grow in amplitude until many modes are present at approximately the same amplitude. At the current of 400 mA, the amplitude of coherent oscillation appears to decrease. Preliminary measurements using a streak camera indicate the bunches lengthen, presumably because of decoherence, thus reducing the centroid motion.

5 LONGITUDINAL COUPLED-BUNCH SATURATION

5.1 Saturation Mechanism

To illustrate the saturation mechanism, consider the simple model of a multi-turn instability shown in Figure 5. A bunch passes through a an RF cavity at turn 0 and excites the single cavity resonance, which then oscillates at its resonant frequency. The cavity frequency has been chosen to be very low for purposes of illustration. On the arrival at the next turn,

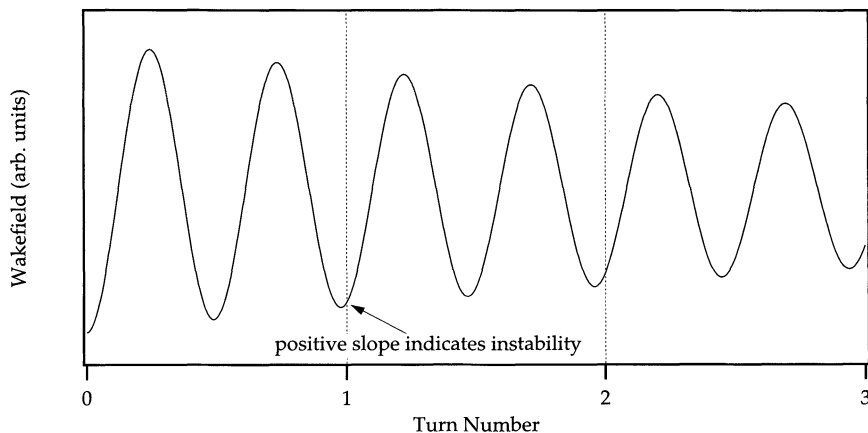


FIGURE 5: Physical picture of saturation mechanism for a multiturn instability. Growth stops when the oscillations approach a half wavelength of the driving wakefield.

the bunch sees either a positive, negative, or zero slope of its own wakefield. It is the sign of the slope which determines whether the oscillation is damped or growing. This is the well-known Robinson instability.

At the onset of the bunch's oscillation growth, the bunch is oscillating over a very small fraction of a period of the wakefield. As the oscillation amplitude becomes comparable to approximately a half period of the wakefield, it samples equally over positive and negative slopes and the resulting destabilizing effect averages to zero and the oscillations do not grow further. An equivalent mathematical description has been given for a single bunch multiturn instability by Krinsky¹² which holds that, to first order, the oscillation limits when the amplitude of phase oscillation at the frequency of the HOM is at the first zero of the zeroth order Bessel function, J_0 . Other saturation mechanisms^{7,10} involving nonlinear Landau damping may be related to the above mechanism and may explain some of the turbulent behavior observed in beam measurements and in simulations. However, this subject is beyond the scope of this paper.

5.2 Numerical Simulations

In order to further study the saturation effect for many bunches and many HOMs under a variety of conditions, a simple numerical tracking code was developed.^{13,14} The variables used to describe the bunch oscillations are the bunch phase at the RF frequency, ϕ , relative to the synchronous phase, and its time derivative, $\dot{\phi}$, which is directly proportional to the deviation from the design energy. The difference equations used are

$$\phi_{i+1} = \phi_i + T_0 \dot{\phi}_i \quad (8)$$

and

$$\dot{\phi}_{i+1} = \left(1 - \frac{2}{\tau_{\text{rad}}}\right) \dot{\phi}_i + \frac{\alpha \omega_{rf}}{E} (eV_c \sin(\phi_{i+1} + \phi_s) + eV_{w,i+1}) \quad (9)$$

where T_0 is the revolution period, V_c is the cavity voltage, ϕ_s is the synchronous phase angle, and V_w is the wake voltage. All other symbols are defined in Table 1. The time evolution of the wake voltage is simplified by treating it as phasor. Its difference equation is given by

$$\tilde{V}_{w,i+1} = \tilde{V}_{w,i} e^{(j\omega_r - \frac{\omega_r}{2Q})\Delta t_i} - \frac{\omega R_{\parallel}}{Q} q \quad (10)$$

where Δt is the time between bunch passages including the effect of the phase oscillation, and q is the bunch charge. Only the real part of \tilde{V}_w is used in Equation 9.

Shown in Figure 6 is the result of a simulation with symmetric fill pattern of 4 bunches under nominal ALS conditions. Only one resonator HOM is used and is purposely tuned to the frequency of an unstable CB mode at approximately 4 times the RF frequency. A high Q HOM is used so that only one CB mode is affected. Figure 6a shows the phase oscillations initially grow with the calculated growth rate until the growth appears to saturate at the expected amplitude. The complex behavior of the phase oscillations subsequent to the initial saturation is not yet understood but is believed to result from the combination of

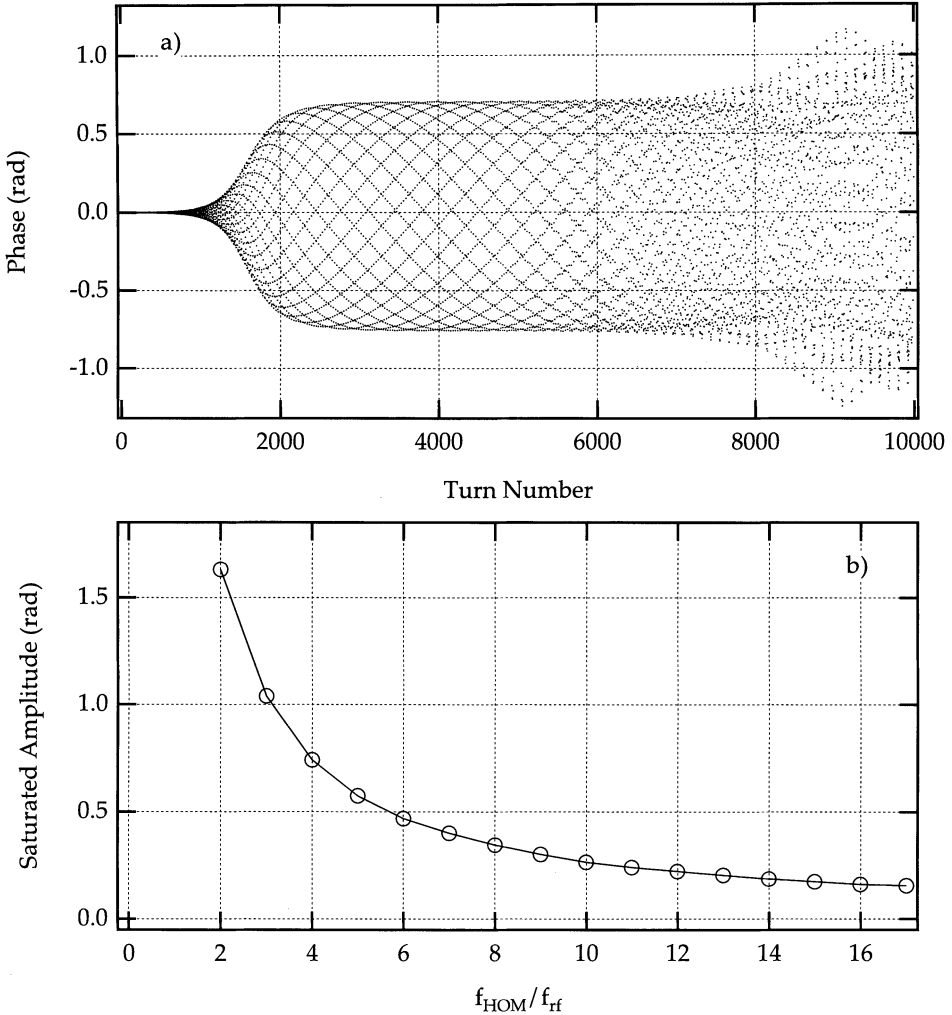


FIGURE 6: Tracking simulation results. (a) Saturation of growth for 4 bunches driven by a single HOM resonator at 4 times the RF frequency. Growth initially limits at $\sim \frac{\pi}{4}$. (b) Saturation amplitude vs. ratio of HOM frequency to RF frequency.

the nonlinearity of wakefield and the the RF voltage. Figure 6b shows the inverse relationship between the initial saturation amplitude and the HOM frequency.

The results of a simulation of ALS conditions with 328 bunches and 9 HOMs using the measured HOM parameters shown in Table 2 is presented in Figure 7. The long term behavior shows limited oscillations with an RMS amplitude of 25 degrees, very similar to measured amplitudes of 20–30 degrees.

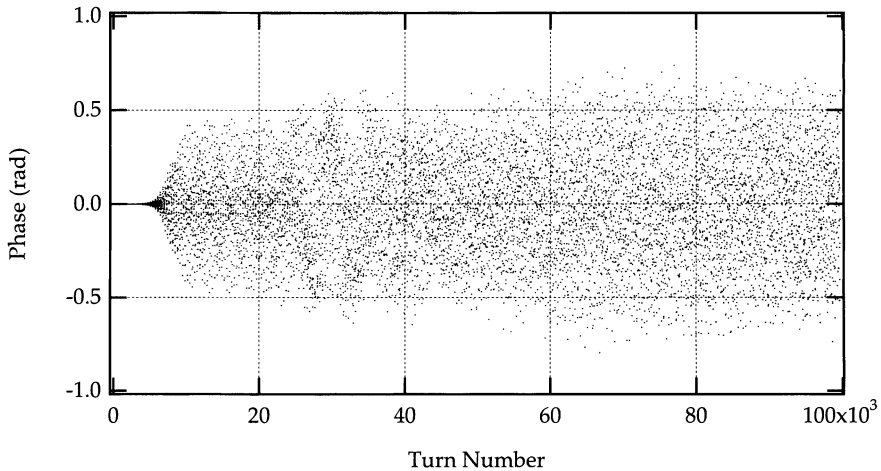


FIGURE 7: Tracking simulation results over many turns for nominal ALS conditions using all measured RF cavity HOM parameters.

6 DISCUSSION AND CONCLUSIONS

We have presented measurements characterizing the longitudinal CB oscillations in the ALS. All of these measurements show good correlation between the unstable CB mode spectrum and the measured HOM impedance of the RF cavities. The stability threshold of the most unstable CB mode is $\sim 5\text{--}10$ mA, close to the predicted stability threshold. The largest CB mode amplitude appears to be limited to ~ 10 degrees at the RF frequency. Individual bunch oscillations are measured to be $\sim 20\text{--}30$ degrees. A feedback system to damp the oscillations¹⁵ is currently in development.

ACKNOWLEDGEMENTS

We would like to thank Glen Lambertson for many useful discussions and the other members of the Center for Beam Physics for their support, and Alan Jackson and the ALS Operations Team for support and assistance. This work was supported by the Director, Office of Energy Research, Office of Basic Energy Sciences, Materials Sciences Division, of the U.S. Department of Energy under Contract No. DE-AC03-76SF00098.

REFERENCES

1. J. Byrd, *to appear in the Proceedings of the 1994 European Particle Accelerator Conference, London.*
2. A. Warwick, personal communication.
3. F. Sacherer, *IEEE Trans. Nucl. Sci. NS-20-3, 825 (1973).*

4. L.J. Laslett, V.K. Neil, and A.M. Sessler, *Rev. Sci. Instrum.* **36**, 426 (1965).
5. T.M. O'Neil, J.H. Winfrey and J.H. Malmberg, *Phys. Fluids*, **14**, 6, 1204, (1971).
6. J. Leclare, *Proceedings of the 11th International Conference on High Energy Accelerators*, (Basel: Birkhauser Verlag, 1980, ed. W.S. Newman).
7. A. Gerasimov, *Phys. Rev. E*, **49**, 2331 (1994).
8. B. Taylor, *et al.*, *Proceedings of the 1993 IEEE Particle Accelerator Conference*, Washington, D.C. (IEEE, New York, 1993) p. 1238.
9. J. Corlett, J. Byrd, *Proceedings of the 1993 IEEE Particle Accelerator Conference*, Washington, D.C. (IEEE, New York, 1993) p. 3408.
10. P. Channell and A. Sessler, *NIM*, **136**, (1976).
11. R. Siemann, in *The Physics of Particle Accelerators*, AIP Conf. Proc. **184**, 431 (1988).
12. S. Krinsky, *Proceedings of the 1985 IEEE Particle Accelerator Conference*, (IEEE, New York, 1993).
13. R. Siemann, *Computer Models of Instabilities in Electron Storage Rings*, in *The Physics of Particle Accelerators*, AIP Conf. Proc. **127**, 431 (1983).
14. K. Thompson, *Proceedings of the 1989 IEEE Particle Accelerator Conf.* (1989).
15. J. Fox, *et al.*, in *Proceedings of the 1993 IEEE Particle Accelerator Conference*, May 1993.